

Benefits of Carrier Pocket Anisotropy to Thermoelectric Performance: The case of p -type AgBiSe_2

David Parker, Andrew F. May and David J. Singh

Oak Ridge National Laboratory, 1 Bethel Valley Rd., Oak Ridge, TN 37831

(Dated: May 14, 2015)

We study theoretically the effects of anisotropy on the thermoelectric performance of p -type AgBiSe_2 . We present an apparent realization of the thermoelectric benefits of one-dimensional “plate-like” carrier pocket anisotropy in the valence band of this material. Based on first principles calculations we find a substantial anisotropy in the electronic structure, likely favorable for thermoelectric performance, in the valence bands of the hexagonal phase of the silver chalcogenide thermoelectric AgBiSe_2 , while the conduction bands are more isotropic, and in our experiments do not attain high performance. AgBiSe_2 has already exhibited a ZT value of 1.5 in a high-temperature disordered fcc phase, but room-temperature performance has not been demonstrated. We develop a theory for the ability of anisotropy to decouple the density-of-states and conductivity effective masses, pointing out the influence of this effect in the high performance thermoelectrics Bi_2Te_3 and PbTe . From our first principles and Boltzmann transport calculations we estimate the performance of p -type AgBiSe_2 .

I. INTRODUCTION

Anisotropy is a substantial contributor to many phenomena of technological importance in condensed matter physics. For example, today’s high performance magnets owe their performance in large part to a sizable magnetocrystalline anisotropy, deriving from spin-orbit coupling, the associated crystal field, and a non-cubic crystal symmetry.

Anisotropy is also important for thermoelectric performance, or the figure-of-merit ZT (defined in Appendix A). Very recently¹ Mecholsky *et al* found that band “warping”, or a non-analyticity of the effective mass tensor near the band edge, can have a substantial effect on the electronic transport relevant for thermoelectric behavior. In that work as well as the recent review by Shakouri² it was pointed out that the existence of a band edge with different masses in different directions favors thermoelectric performance. This was also shown in Ref. 3, and the benefits of anisotropy to thermoelectric transport, with regards to FeAs_2 and LiRh_2O_4 , were shown in Refs. 4 and 5. In fact this basic scenario, applied to artificial structures, had been foreseen by Hicks and Dresselhaus^{6,7} in works on thermoelectric transport in superlattices and nanowires. It was also shown⁸ that one can realize the beneficial effects of low-dimensional *electronic* structures even in isotropic materials.

Numerous authors have noted^{9–19} the effect of carrier pocket degeneracy on thermoelectric performance, noting that such degeneracy improves electrical conductivity without sacrificing the Seebeck coefficient, both indispensable components of a useful thermoelectric. Such degeneracy is nearly universally rooted in the placement of a band extremum away from the Γ point since the crystal symmetry then dictates the appearance of multiple carrier pockets. This crystal symmetry also ensures that anisotropy in the electronic transport resulting from a single carrier pocket, which we term “pocket anisotropy”, does not sacrifice the *overall* electronic transport of the crystal. Examples of such pocket anisotropy include the valence bands of the high performance thermoelectrics Bi_2Te_3 and PbTe . The valence bands of both these materials contain band edges away from the Γ point with three²⁰ (for Bi_2Te_3) and two²¹ (for PbTe) disparate effective masses in different directions. However, the transport is isotropic in the basal plane

for Bi_2Te_3 and for all three dimensions in cubic PbTe . Our calculations described below find essentially isotropic *overall* electrical transport for p -type AgBiSe_2 despite substantial *carrier pocket* anisotropy.

In addition, the benefits of mass anisotropy increase as the dimensionality of the electronic structure decreases. For example, an isotropic three dimensional parabolic band has a \sqrt{E} dependence of the density-of-states $N(E)$ on energy E , a two-dimensional parabolic band has a step-function behavior, and a fully one-dimensional band has an $E^{-1/2}$ behavior, implying a diverging density-of-states (DOS) at the band edge. Note that a one-dimensional band takes on a “sheet” or “plate-like” isoenergy or Fermi surface. While in real materials such a DOS divergence does not occur due to a lack of complete one-dimensionality, it is clear there are particular benefits of such a one-dimensional structure.

In this work we present calculations of such one-dimensional “plate-like” carrier pocket anisotropy in the valence band of the silver chalcogenide semiconductor AgBiSe_2 . This material crystallizes in a hexagonal structure at room temperature, with successive transitions to a rhombohedral structure at 420 K and to a disordered fcc structure at about 600 K. Recent work^{22–24} shows a ZT value for n -type AgBiSe_2 of 1.5 just above the cubic-rhombohedral phase transition. We find from theory that good room-temperature p -type thermoelectric performance may be possible, estimating a p -type ZT value of 0.4–0.7, considering only electronic optimization.

Ordinarily one-dimensional electronic structures are associated with electronic instabilities such as charge or spin-density waves. These instabilities typically lead to insulating ground state behavior. Here, by contrast, we have a one-dimensional electronic structure⁴ associated with a *metallic* ground state, that we will show to be highly beneficial for thermoelectric performance.

We observe that very few materials have $ZT \sim 1$ in the important temperature range between 200 and 350 K, where many heating and cooling applications exist. Substantial efforts to find a substitute for the prototypical thermoelectric Bi_2Te_3 , which shows a ZT of unity around room temperature, have been made for nearly 50 years. Hence the finding of a candidate for such performance levels, assuming full

optimization, in this temperature range is of substantial importance. This remains true even despite the difficulty, described below, of doping into the valence band of AgBiSe₂. We note that both Bi₂Te₃ and AgBiSe₂ contain expensive elements (Tellurium and Silver). However, Silver is more available, with worldwide annual production is 26,000 tons, compared to Tellurium, with annual production of 100 tons²⁵. This parallels the 75 times larger mass abundance²⁶ in the Earth's crust of Silver relative to Tellurium.

The remainder of this paper is organized as follows: in Section II, we present our experimental procedure; in Section III we present our experimental data, along with a comparison of the calculated *n*-type and *p*-type electronic structures; in Section IV, we present a more general consideration of anisotropy, followed in Section V with our first principles theoretical results and our estimate of *ZT*, and our conclusions in Section VI. Details on the estimation of *ZT* are presented in Appendix A, and a demonstration of the isotropy of the Seebeck coefficient within an effective mass approach is given in Appendix B.

II. EXPERIMENTAL PROCEDURE AND EFFORTS TO ATTAIN *p*-TYPE DOPING

AgBiSe₂ samples were prepared by reacting high-purity elements in evacuated silica ampoules. For the 'as-grown' sample, solidification occurred slowly (1 deg/hr) to promote large grains. The sample was then cooled at 5deg/hr between 310°C and 260°C, followed by a 48h anneal at 260°C to minimize defects and reduce residual stresses. Due to the formation of voids during growth and cracks during processing, only relatively small pieces were obtained. These difficulties lead to the synthesis of polycrystalline samples, which also allow for a more rapid screening of potential dopants. Following reaction in the melt, samples were ground in a He glove box and hot-pressed in a graphite die at temperatures near 450°C with a pressure of approximately 10,000 psi. This process resulted in samples with geometric densities of approximately 95% of the theoretical density.

The Seebeck coefficient was used as a screening tool to examine the influence of the various substitutions and processing conditions. The Seebeck and Hall coefficients were measured in a Quantum Design Physical Property Measurement System, using the Thermal Transport and Resistivity Options, respectively. Thermal measurements were performed using gold-coated copper leads attached to the sample with H20E Epo-Tek silver epoxy. Hall data were obtained using a standard four-wire configuration, with 0.0508 mm Pt wires spot welded to the sample and maximum fields of ± 6 T were employed; electrical resistivity was collected during the same measurement as the Seebeck coefficient and thermal conductivity. Scanning electron microscopy (SEM) and energy dispersive spectroscopy (EDS) measurements were performed in a Hitachi TM-3000 microscope equipped with a Bruker Quantax 70 EDS system.

In order to manipulate the electrical properties, polycrystalline samples containing S, Te, and Pb were made. Sim-

ilarly, a sample of nominal composition Ag_{1.1}Bi_{0.9}Se₂ was produced from the melt to examine the potential for intrinsic hole doping via bismuth deficiency. SEM coupled with EDS revealed a Ag-rich phase at apparent grain boundaries in this Ag_{1.1}Bi_{0.9}Se₂ sample, which indicates the tendency of the phase to form near the stoichiometric composition AgBiSe₂. This sample was not considered further due to our desire to probe, as much as possible, only the intrinsic properties of AgBiSe₂.

In our experimental results, AgBiSe₂ naturally forms *n*-type. As-grown AgBiSe₂ was found to have a Hall carrier density n_H near $2.3 \times 10^{19} \text{cm}^{-3}$ at room temperature, and little temperature variation was observed down to 25K. At 300 K, this as-grown sample had a Seebeck coefficient of $-138 \mu\text{V/K}$ and a Hall mobility of $\mu_H = 45 \text{cm}^2/\text{V/s}$. Our polycrystalline AgBiSe₂ had a Seebeck coefficient of $\approx -400 \mu\text{V/K}$ at 300 K, and an electrical resistivity that increased with decreasing temperature. These results suggest that our polycrystalline AgBiSe₂ is very lightly doped, or nearly an intrinsic semiconductor. Thus, AgBiSe₂ can be formed near the insulating limit, which makes obtaining *p*-type conduction more plausible.

Pb has previously been shown²² to induce *p*-type conduction in AgBiSe₂. However, our Pb-doped sample of nominal composition AgBi_{0.95}Pb_{0.05}Se₂ had a Seebeck coefficient of $\approx -95 \mu\text{V/K}$, suggesting a higher electron concentration than the as-grown sample or the polycrystalline AgBiSe₂. The apparent increase in free electrons with a *p*-type dopant is surprising, and may be related to inhomogeneities within the sample. However, the absence of *p*-type conduction at low Pb concentrations was reported by Pan et al²², though they observed a cross-over to *p*-type conduction near $x = 0.02$. We did not continue to investigate Pb-doping after this initial finding. Instead, we briefly examined the influence of S and Te substitutions.

The *n*-type behavior of AgBiSe₂ may be caused by Se vacancies. To gain insight into this potential mechanism, we considered S and Te substitutions for Se. Interestingly, our sample of nominal composition AgBiSe_{1.8}Te_{0.2} had a room temperature Seebeck coefficient of $-475 \mu\text{V/K}$ and resistivity that increased with decreasing *T*. Compared to the $-400 \mu\text{V/K}$ observed for the undoped, polycrystalline sample, this would suggest that Te substitution drives the systems towards a charge balanced state due to its lower vapor pressure (fewer anion vacancies). However, we remain cautious because AgBiTe₂ is also naturally *n*-type²⁷. Also, Seebeck coefficient measurements become more difficult and absolute errors increase for resistive samples. Yet, sulfur substitution pushed the system in the opposite direction (more metallic), consistent with a relative increase in elemental vapor pressure. Unfortunately, there was no trend in these data and the more heavily substituted sample had a larger 300 K *n*-type Seebeck coefficient ($-87 \mu\text{V/K}$ for 5% S, and $-175 \mu\text{V/K}$ for 10% S). As such, we cannot draw any conclusions regarding the sulfur substitution, though we remain optimistic about coupling Te substitution with non-isoelectronic dopants.

A detailed study of the defect chemistry in these materials could provide the insights required to achieve the desired

levels of p -type conduction. A more complete picture would require additional experimental and theoretical efforts, considering the variety of compositions in this family of I-V-VI₂ chalcogenides.

The large Seebeck coefficients and semiconducting behavior of the resistivity of our polycrystalline samples thus suggest that an adequate p -type dopant might be found. We also note that in Refs. 23 and 24 p -type behavior - i.e. positive Seebeck coefficient - was observed in the low-temperature hexagonal phase, so our results should not be taken to imply that p -type doping is impossible to achieve in AgBiSe₂, merely that more involved effort will likely be required to achieve this. In the literature there are numerous semiconductors such as CrSi₂ and Bi₂Se₃^{28,29} which were originally found to exhibit a strong doping type preference, which were later found possible to dope both n -type and p -type under the proper circumstances. Since AgBiSe₂ has not undergone much experimental study to date, we think it likely that the difficulty in attaining p -type doping will be successfully addressed by future efforts. We note finally that the relatively narrow calculated band gap of 0.52 eV (see Section IV) argues in favor of the likelihood of attaining both doping types.

III. EXPERIMENTAL DATA AND THEORETICAL COMPARISON OF n -TYPE AND p -TYPE

In Figure 1 we show the T -dependent Seebeck coefficient, resistivity and thermal conductivity for the as-grown sample, along with (left panel) our first principles calculation of the Seebeck coefficient for this sample. The measured Hall number, $-0.27 \text{ cm}^3/\text{Coul}$, would correspond to an electron concentration n of $2.3 \times 10^{19} \text{ cm}^{-3}$ in the case of an isotropic parabolic band, although Fig. 2 (top) depicts a conduction band electronic structure significantly differing from isotropic, so that the chemical and Hall-inferred carrier concentrations may differ. We find a good fit at a *chemical* carrier concentration n of $2.52 \times 10^{19} \text{ cm}^{-3}$ indicating the accuracy of our theoretical approach, which uses the constant scattering time approximation³⁰.

The right hand panel of Fig. 1 shows the thermal conductivity and resistivity measurements. We see that the thermal conductivity κ of AgBiSe₂ is extremely low - it reaches a minimum value of 1.1 W/m-K around 200 K, indicating low lattice thermal conductivity - a key parameter of a useful thermoelectric. In fact, using the resistivity data and the Wiedemann-Franz relationship we find the lattice term at 200 K to be just 1.0 W/m-K , which is lower than that of the better-known high performance thermoelectrics such as Bi₂Te₃ and PbTe. This value is slightly higher than that found by Nielsen *et al* for rhombohedral AgBiSe₂³¹, presumably due to the difference in physical structure. The slight upturn of κ above 200 K likely reflects radiative effects not corrected for here.

The resistivity data shows the Fermi-liquid T^2 dependence at the very lowest temperatures below 50 K, crossing over to T -linear behavior for temperatures above 100 K. This T -linear behavior is characteristic of electron-phonon scattering and allows us to estimate the electron phonon coupling constant λ

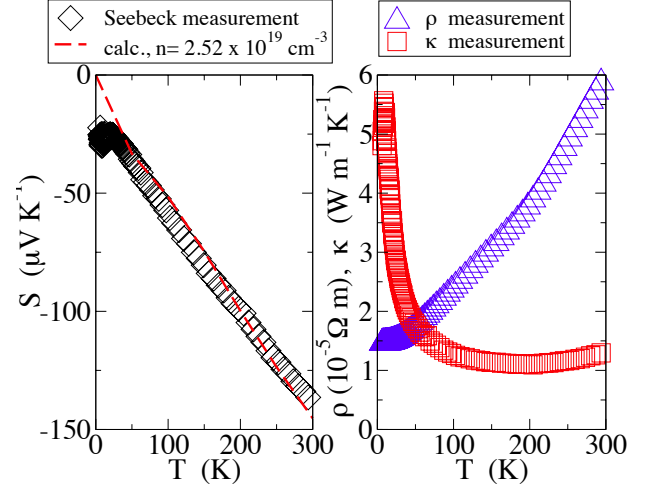


FIG. 1. (Left panel) The measured and calculated thermopower of AgBiSe₂; right panel, the measured resistivity (blue triangles) and thermal conductivity (red squares).

for this sample. We will later use this to estimate the performance of p -type AgBiSe₂. From our theoretical calculations we find the plasma frequency squared ω_p^2 at the modeled doping level to be 0.096 eV^2 . When we combine this with our resistivity data and the theoretical relationship connecting λ , ω_p , and the resistivity from Ref. 32, we find an electron-phonon coupling constant of 0.49, and an associated electronic scattering time of $8 \times 10^{-15} \text{ s}$.

Although we were able to obtain significant n -type doping levels, our data suggest that in this temperature range n -type AgBiSe₂ is not likely to be a high performance thermoelectric. The 300 K power factor $S^2\sigma$ for our as-grown sample is just 0.3 mW/m-K^2 , or less than 10 percent of the value of optimized Bi₂Te₂. Although one might achieve some gain in the power factor in a more lightly doped sample, this will not likely raise 300 K ZT substantially from the ~ 0.1 value achieved here (a rough estimate finds optimized ZT values of less than 0.2).

It is of interest to understand the reason for this. Presented in Figure 2 (top) is a plot of the first-principles calculated isoenergy surface for n -type AgBiSe₂ for a doping $n = 1.23 \times 10^{20} \text{ cm}^{-3}$. The plot depicts a cylindrical body whose width is quite comparable to its height. While the cylindrical surface is suggestive of two-dimensionality and hence mass anisotropy, the *shape* does not lend itself to a large surface to volume ratio, which we have argued elsewhere³ to be favorable for high ZT . The structure is also substantially lacking in degeneracy (technically there is a two-fold degeneracy as the band edge is at the A point). Given these factors and the lack of the favorable complexity described in Ref. 33, it is perhaps not surprising that the performance levels of hexagonal n -type AgBiSe₂ are comparatively low.

The situation is rather different for p -type, however. Figure 2 (bottom) presents a plot of the isoenergy surface for p -type AgBiSe₂ at the same carrier concentration as depicted for n -

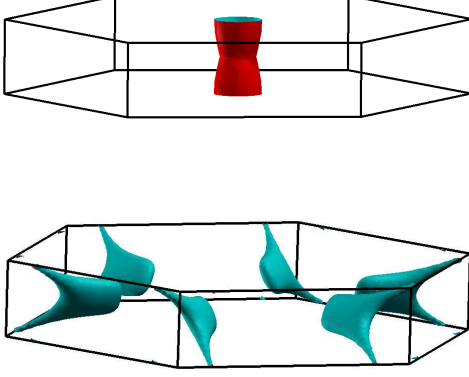


FIG. 2. The calculated Fermi surface of hexagonal AgBiSe₂ at an electron doping $n = 1.23 \times 10^{20} \text{cm}^{-3}$ (top) and the same carrier concentration for p -type (bottom). The bottom plot is rotated slightly to better depict the degeneracy and mass anisotropy.

type. This doping is likely near the optimal p -type doping for room-temperature ZT . The Fermi surface consists of six platelike structures that exhibit the feature mentioned in the Introduction: a perpendicular mass much less than the parallel mass. In fact, in the plane of the “plate”, the effective mass is approximately 5 times the perpendicular mass. There are additionally highly elongated features which stretch out to a secondary band maximum at a non-symmetry point on the zone surface. We also note the six-fold degeneracy, a combination of the hexagonal symmetry and the position of the VBM away from Γ , and away from high-symmetry zone boundary positions. Finally, one observes the *orientation* of the “plates”: they are located at an angle to the c -axis, not parallel to it, so that the favorable transport properties of this feature will extend to the c -axis transport as well. We will see that p -type transport in this material is expected to be virtually isotropic.

In the next section we give a general theoretical description of the benefits of carrier pocket anisotropy in enhancing thermoelectric performance, as appear to be active in p -type AgBiSe₂, specifically the role of such pocket anisotropy in decoupling the *density-of-states* or thermopower effective mass from the *conductivity* effective mass.

IV. THEORY OF ROLE OF POCKET ANISOTROPY IN DECOUPLING DENSITY-OF-STATES AND CONDUCTIVITY EFFECTIVE MASSES

Here we show that any semiconductor band edge pocket anisotropy that can be expressed in terms of an ellipsoidal effective mass tensor has substantial benefits to thermoelectric performance, provided that the band edge is not located at the Γ point and the crystal obeys a certain minimum symmetry. Larger anisotropies, in addition to the effects of band degeneracy⁹, are shown to be more beneficial in this regard.

We begin with the canonical expressions for the temper-

ature and chemical-potential-dependent thermopower tensor $S_{\alpha\alpha}(T, \mu)$ and the electrical conductivity tensor $\sigma_{\alpha\alpha}(T, \mu)$, which we reproduce here from Ref. 36. For simplicity we assume that both are diagonal in the spatial indices α and also assume only one band contributes to transport. Then we have:

$$S_{\alpha\alpha}(T, \mu) = \frac{v_{\alpha\alpha}(T, \mu)}{\sigma_{\alpha\alpha}(T, \mu)} \quad (1)$$

with

$$\sigma_{\alpha\alpha}(T, \mu) = - \int \sigma_{\alpha\alpha}(E) \frac{\partial f(T, E)}{\partial E} dE \quad (2)$$

and

$$v_{\alpha,\alpha}(T, \mu) = \frac{-1}{eT} \int \sigma_{\alpha\alpha}(E) (E - \mu) \frac{\partial f(T, E)}{\partial E} dE \quad (3)$$

Here $\sigma_{\alpha,\beta}(E)$ is the transport function which is written as

$$\sigma_{\alpha\alpha}(E) = e^2 \sum_{i,\mathbf{k}} v_{\mathbf{k},\alpha,i}^2 \tau_{i,\mathbf{k}} \delta(E - E_{i,\mathbf{k}}) \quad (4)$$

and f is the Fermi function. Note that for an anisotropic parabolic band, in which the relaxation time τ depends on \mathbf{k} through $E_{i,\mathbf{k}}$, the above expression (Eq. 4) for the transport function can be written as

$$\sigma_{\alpha,\alpha}(E) = e^2 v_{\alpha}^2(E) \tau_{\alpha}(E) N(E) \quad (5)$$

Here the effective mass anisotropy is incorporated into the directional index α .

As described in Appendix B, this effective mass anisotropy nonetheless yields an isotropic Seebeck coefficient, so long as the bands are taken as parabolic, only carriers of one sign contribute to transport, and the scattering time is taken as depending only on energy, not on direction. We note also that, though difficult to obtain in practice, a highly anisotropic Seebeck coefficient is of interest in the study of transverse thermoelectric effects³⁷.

We now analyze this problem through the concept of effective mass. From standard references³⁸ the electrical conductivity tensor may be written as

$$\sigma = \tau \sum \frac{d^3 k}{4\pi^3} \mathbf{M}^{-1} \quad (6)$$

where \mathbf{M}^{-1} is an effective mass tensor and the sum is taken over occupied levels. The standard electronic conductivity formula (where we have retained the directional indices) can then be written as

$$\sigma_{\alpha,\alpha} = \frac{ne^2 \tau_{\alpha}}{m_{\sigma,\alpha}} \quad (7)$$

and contains a conductivity effective mass $m_{\sigma,\alpha}$ to which the conductivity is inversely proportional. For high electrical conductivity (a prerequisite for good thermoelectric performance) one therefore desires small effective masses, irrespective of the scattering time τ_i .

The situation is very different for the thermopower S . In the fully degenerate limit the Mott formula gives the thermopower as

$$S_{\alpha,\alpha}(n, T) = \frac{\pi^2}{3} \frac{k_B}{e} k_B T \left(\frac{d \log(\sigma_{\alpha\alpha}(E))}{dE} \right) \Big|_{E=E_F} \quad (8)$$

For an anisotropic parabolic band, one has (from Appendix B) that

$$\sigma_{\alpha\alpha}(E) = g_{3,\alpha}(m_x, m_y, m_z)E^{3/2} \quad (9)$$

where E is measured from the band edge and g_3 is a function of the band masses. The logarithmic derivative in the above equation is simply $3/2E_F$. E_F may be rewritten in terms of the carrier concentration n and effective masses m_x, m_y and m_z by noting that n can be written as (using the formula for the volume of an ellipsoid and including a factor of 2 for spin degeneracy)

$$n = \frac{2}{(2\pi)^3} \frac{4\pi}{3} k_{F,x} k_{F,y} k_{F,z} \quad (10)$$

where $\hbar k_{F,i} = \sqrt{2m_i E_F}$ with m_i the effective mass in direction i , yielding

$$n = \frac{1}{3\pi^2 \hbar^3} \sqrt{8m_x m_y m_z} E_F^{3/2} \quad (11)$$

Combining the above equations and rewriting $(m_x m_y m_z)^{1/3}$ as m_{DOS} , we finally have

$$S(T, n) = \frac{4\pi^2 k_B^2}{eh^2} m_{DOS} T \left(\frac{4\pi}{3n} \right)^{2/3} \quad (12)$$

For the thermopower larger effective DOS masses are beneficial, which runs completely counter to the benefit to the conductivity of smaller masses. This is one major fundamental problem that must be overcome to achieve high thermoelectric performance.

However, as suggested by the notation, *there is no particular reason that m_σ and m_{DOS} must be equal*. They are in fact equal only for a single isotropic parabolic band. This distinction is well-known for the case of band degeneracy, where a band edge of degeneracy N enhances⁹ m_{DOS} by a factor $N^{2/3}$ without affecting m_σ . Here we explore in addition the effect of anisotropy on the relation of these two masses. We find that anisotropy allows for small *conductivity* effective masses m_σ , heightening the electronic conductivity, but large *density-of-states* effective masses m_{DOS} , enhancing the thermopower.

One can see the reason for this quite easily. For simplicity, (the effect is similar for three distinct masses) consider an anisotropic parabolic band edge represented by a three-dimensional ellipsoid of revolution, characterized by two effective masses, a radial mass m_\parallel and a longitudinal mass m_\perp . The DOS effective mass for this situation is given by $m_{DOS} = (m_\parallel^2 m_\perp)^{1/3}$. The conductivity effective masses in each of the two directions are given by m_\parallel and m_\perp . However, for a crystal in which the band edge is not at the Γ , or similarly low-degeneracy, point, there will generally be some band edge degeneracy which respects the crystal symmetry. As depicted in Ref. 8, this means that even an anisotropic band edge can result in isotropic transport in a cubic material. The same general idea applies for planar transport for a layered material such as Bi_2Te_3 . One then sees that the (isotropic) conductivity effective mass is given by

$$3/m_\sigma = 2/m_\parallel + 1/m_\perp \quad (13)$$

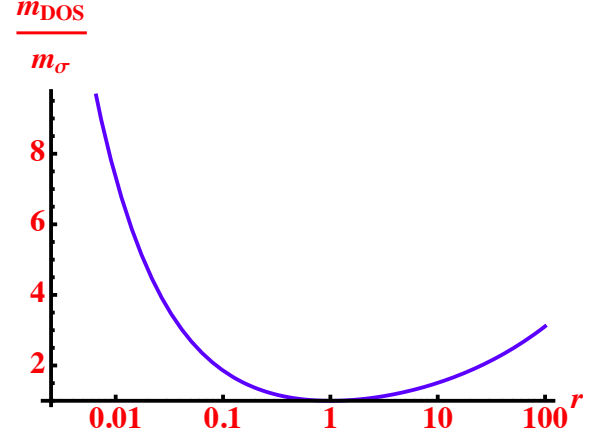


FIG. 3. The ratio m_{DOS}/m_σ . Here $r = m_\perp/m_\parallel$.

so that

$$m_\sigma = \frac{3m_\parallel m_\perp}{2m_\perp + m_\parallel} \quad (14)$$

As is clear from the expression, this conductivity mass m_σ has a rather different dependence on m_\perp and m_\parallel than the density-of-states mass m_{DOS} . Indeed, the ratio m_{DOS}/m_σ , which is effectively a figure-of-merit for the effects of electronic anisotropy, is simply

$$m_{DOS}/m_\sigma = \frac{2m_\perp + m_\parallel}{3(m_\parallel m_\perp^2)^{1/3}} \quad (15)$$

$$= (2/3)r^{1/3} + (1/3)r^{-2/3} \quad (16)$$

In the last expression we have expressed m_{DOS}/m_σ in terms of r where r is the mass ratio m_\perp/m_\parallel . Now, this m_{DOS}/m_σ ratio can be substantially different from unity if m_\parallel and m_\perp are very different. For a case where $m_\perp = 24m_\parallel$ (a value present in the conduction band of GeTe ³, this ratio approaches the value 2. Additionally, in the opposite limit, in which the band edge forms a flattened, highly prolate, rather than oblate, spheroid, still larger effects are present. Figure 3 depicts a plot of the DOS to conductivity mass ratio as a function of the ratio $r = m_\perp/m_\parallel$. For this ratio = 1/100 one finds a DOS to conductivity mass ratio of nearly 10, which is clearly beneficial in enhancing both thermopower and electrical conductivity.

As examples of these concepts, we consider the p -type band masses in the high performance thermoelectrics Bi_2Te_3 and PbTe . The band edge in p -type Bi_2Te_3 has three distinct masses²⁰, which take the values of $0.064 m_0$, $0.196 m_0$, and $0.73 m_0$, where m_0 is the free electron mass. These yield a band edge m_{DOS} of $0.209 m_0$ and m_σ of 0.136 ³⁴ so that their ratio is over 50 percent enhanced relative to an isotropic band edge. When one includes the six-fold degeneracy of the band edge in the DOS mass the effective mass ratio becomes 3.87, which is surely a major contributor to the performance of this material. Similarly, the L-point band edge in PbTe contains a radial mass²¹ of $0.022 m_0$ and longitudinal mass $0.31 m_0$,

yielding an m_{DOS}/m_{σ} of 1.66, or 4.19 if the fourfold L-point degeneracy is included, which likely contributes to the exceptional thermoelectric performance³⁵ of this material.

V. POSSIBLE REALIZATION OF BENEFICIAL EFFECTS OF CARRIER POCKET ANISOTROPY: *p*-TYPE AgBiSe_2

We focus here on the low temperature hexagonal phase of AgBiSe_2 , calculating its properties with the first principles density functional theory code WIEN2K³⁹, as well as Boltzmann transport properties via the Boltztrap code⁴⁰, within the generalized gradient approximation (GGA) of Perdew, Burke and Ernzerhof⁴¹. For these calculations we use a modification of the GGA known as a modified Becke Johnson potential⁴² which gives accurate band gaps^{43,44}, a matter of great importance for the transport properties. The linearized augmented plane wave (LAPW) basis was used, with LAPW sphere radii of 2.5 Bohr for all atoms, and an RK_{max} of 9.0 was used. Here RK_{max} is the product of the sphere radius and the largest basis wave vector. Approximately 1000 k -points in the full Brillouin zone were used for the self-consistent calculations run to convergence and approximately 10,000 points were used for the transport calculations. The internal coordinates were relaxed using the standard GGA until forces were less than 2 mRyd/bohr. All other calculations, the relaxations excepted, included spin-orbit.

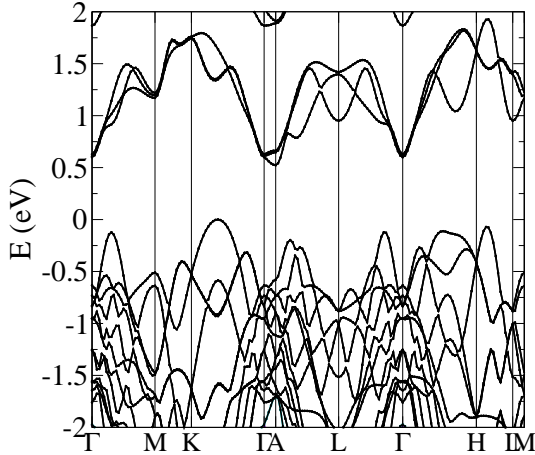


FIG. 4. The calculated band structure of hexagonal AgBiSe_2 .

Figure 4 depicts the calculated band structure of hexagonal AgBiSe_2 . From the figure, we see that this material is a semiconductor of band gap 0.52 eV, with conduction band minimum at the A point and a valence band maximum located between the Γ and K points (the Brillouin zone for these points is found in Ref. 45). The valence band, in addition contains substantial degeneracy, with at least four subsidiary maxima less than 100 meV from the band edge. These maxima all originate from the same general Fermi surface structure, and in addition we note a wide range of masses for these maxima, with the maximum between Γ and H having the heaviest mass and the adjacent maximum between H and L having the lightest.

This accords with the discussion in the Introduction regarding the anisotropy in band extrema. To demonstrate the potential of this material for high ZT , in Figure 5 we present a plot of the 300 K calculated power factor vs. carrier concentration σ/τ and compare with *p*-type Bi_2Te_3 , the highest performing room temperature thermoelectric. Although the *p*-type thermopower and conductivity of AgBiSe_2 are nearly isotropic, Bi_2Te_3 has substantial anisotropy, as is well known. To ensure a fair comparison we present the conductivity-averaged quantities (see Ref. 3 for details on these quantities) since in a typical experiment a polycrystalline sample is used, which tends to average the transport over the principal axes.

The figure depicts $S^2\sigma/\tau$ results much larger than those of Bi_2Te_3 . In particular, at the doping where the thermopower is $200 \mu\text{V/K}$ (indicated by the asterisks), the $S^2\sigma/\tau$ of AgBiSe_2 is *double* that of Bi_2Te_3 . This doping, which is $p = 2 \times 10^{19} \text{ cm}^{-3}$ for Bi_2Te_3 and $1.2 \times 10^{20} \text{ cm}^{-3}$ for AgBiSe_2 , is approximately the doping of optimized ZT for Bi_2Te_3 and is probably at or near optimal for AgBiSe_2 . While one cannot exclude

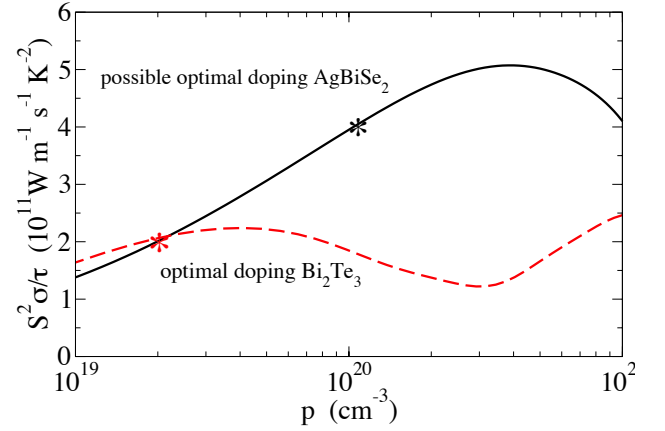


FIG. 5. The calculated power factor divided by scattering time, $S^2\sigma/\tau$ of *p*-type Bi_2Te_3 and AgBiSe_2 . The asterisks indicate the doping where the calculated thermopower is $200 \mu\text{V/K}$, which is usually near the optimal doping for a high performance thermoelectric.

scattering time differences from the comparison, this result suggests that AgBiSe_2 may show comparable power factors to those of Bi_2Te_3 , and when combined with the observed low lattice thermal conductivity of AgBiSe_2 ⁴⁶ suggests a high potential for room-temperature thermoelectric performance.

In Figure 6 we depict the calculated thermopower for AgBiSe_2 as a function of carrier concentration. Note that the *p*-type thermopower is virtually isotropic. We have indicated the range of thermopowers between 200 and $300 \mu\text{V/K}$ as this is the general range of thermopower over which ZT is maximized. From this we find optimal 300 K *p*-type doping levels of $3 \times 10^{19} - 1.3 \times 10^{20} \text{ cm}^{-3}$. For *n*-type the optimal doping levels are much lower, indicating a lower likelihood of good thermoelectric performance.

In Figure 7 we present the calculated 300 K electrical con-

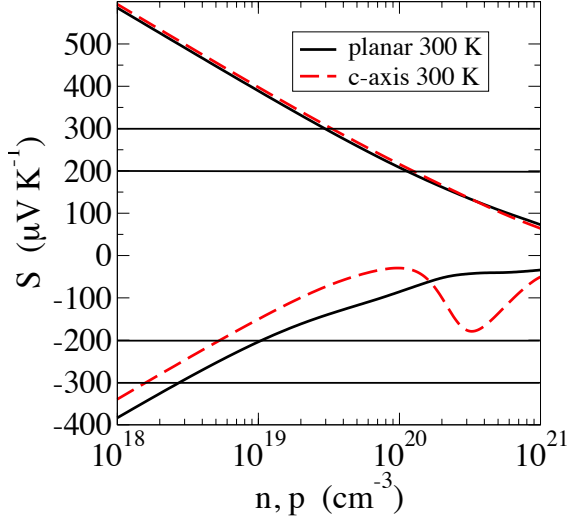


FIG. 6. The calculated thermopower of hexagonal AgBiSe₂ at 300 K.

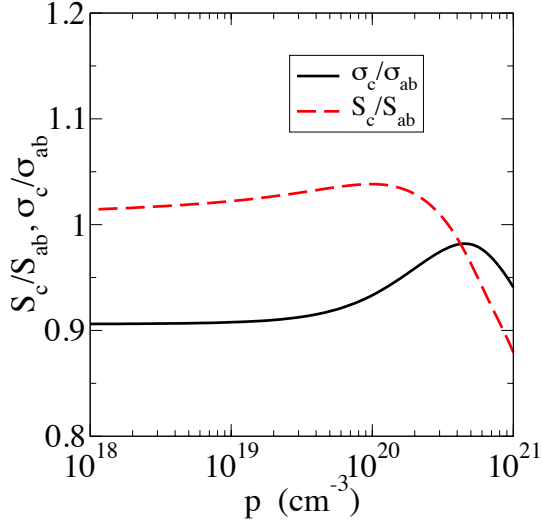


FIG. 7. The calculated electrical conductivity ratio σ_c/σ_{ab} and thermopower ratio S_c/S_{ab} of hexagonal AgBiSe₂ at 300 K.

ductivity and thermopower ratios σ_c/σ_{ab} and S_c/S_{ab} . In view of the great *carrier pocket* anisotropy depicted in Figure 2 (bottom), it is of interest that the thermopower and electrical conductivity of *p*-type AgBiSe₂ vary by no more than 10 percent from the *c*-axis to the plane. Note that the electrical conductivity, with respect to an unknown scattering time τ , is calculated as the transport function $N(E)v_i^2(E)$ integrated with the derivative of the Fermi function, a function sharply peaked around E_F . Here $N(E)$ is the density of states and v_i the Fermi velocity in direction i . Hence the anisotropy of the

conductivity is a good measure of the anisotropy of the transport function itself.

We note that, as suggested by Figures 6 and 7, in general the overall *global* electronic transport anisotropy need not be as large as the *local* carrier pocket anisotropy. Only in the case of a single band extremum are these two anisotropies equal. When multiple extrema, as depicted in the bottom panel of Figure 2, are present the overall anisotropy can be much less than the carrier pocket anisotropy, due to the varying relative orientations of the band extrema dictated by the crystal symmetry. Thus despite the great variation in directional effective mass in the hole pockets in the bottom of Figure 2, the overall electronic transport in *p*-type AgBiSe₂ is very nearly isotropic.

Actual values of the electrical conductivity depend on the electronic scattering time τ , which can vary substantially both from one material to another and by doping level within a particular material. As is well known, for temperatures above the Debye temperature³² τ is generally inversely proportional to the dimensionless electron-phonon coupling constant λ , assuming the absence of extrinsic factors such as grain boundary scattering. While λ is not directly available from the first principles calculations we have performed, we estimated above its value as 0.49 from experimental measurements described in Section II. This section also presented measurements of the thermal conductivity, which allows estimation of the potential *ZT* of *p*-type AgBiSe₂.

As described in Appendix A, from these data we estimate the 300 K *ZT* value of optimally doped *p*-type AgBiSe₂ as 0.4 - 0.7. These values consider only optimization of the electronic transport; optimization of the lattice transport can be expected to yield additional performance benefits. These promising performance values are representative of the positive effects of carrier pocket electronic anisotropy in producing favorable thermoelectric behavior.

VI. CONCLUSION

Carrier pocket electronic anisotropy is seen to positively impact thermoelectric performance, provided that the crystal obeys a minimum symmetry and the relevant band edge is located away from the Γ point so that the material can experience the beneficial effects of both band degeneracy and a large effective mass *ratio* in the ellipsoidal effective mass tensor. *p*-type AgBiSe₂ appears to be a material in which these benefits are present, with “plate-shaped” Fermi surfaces, a large predicted power factor and ultimately a predicted 300 K *ZT* value of 0.4 - 0.7, considering only optimization of the electronic properties. The favorability of this material suggests that other materials with such anisotropic features may exist; indeed, two of the best performing thermoelectrics Bi₂Te₃ and PbTe, exhibit a great deal of such anisotropy. Searches for other potentially high performance thermoelectrics with these anisotropic behaviors may therefore be of interest.

Appendix A : Method for estimation of thermoelectric performance of p -type AgBiSe_2

Thermoelectric performance is measured as

$$ZT = \frac{S^2 \sigma T}{\kappa} \quad (17)$$

Here S is the Seebeck coefficient, κ the thermal conductivity, and σ the electrical conductivity. To make quantitative estimation of thermoelectric performance we need the values of these three quantities. We do this using a combination of our first principles calculations, the experimental data just described, and a few assumptions.

Although in p -type AgBiSe_2 the Seebeck coefficient and electrical conductivity are calculated to be essentially isotropic, we describe here briefly the application of Eq. (17) in the anisotropic case. For a single crystal sample, the above expression for ZT directly applies for the Seebeck coefficient, electrical and thermal conductivity measured in a particular direction, leading to a value of ZT which is directionally dependent. The more typical situation, as in our experimental work, is that of a polycrystalline sample with random grain orientation. In that case ZT of the sample is isotropic, and the values of S and σ which enter the ZT expression are as follows (we assume diagonal S and σ tensors):

$$S = \frac{S_{xx}\sigma_{xx} + S_{yy}\sigma_{yy} + S_{zz}\sigma_{zz}}{\sigma_{avg}} \quad (18)$$

$$\sigma_{avg} \equiv \sigma = \frac{\sigma_{xx} + \sigma_{yy} + \sigma_{zz}}{3} \quad (19)$$

Note that the above expression neglects extrinsic effects such as grain boundary scattering that may reduce σ_{avg} from the average of the corresponding single-crystal direction-dependent conductivities. A detailed consideration of the effect of transport anisotropy on ZT may be found in Ref. 47.

Returning to calculating the ZT of p -type AgBiSe_2 , our first assumption is regarding optimal doping. Rather than estimate the doping dependence of thermoelectric performance, we note that in most high performance thermoelectrics, the Seebeck coefficient magnitude at optimal doping is between 200 and 300 $\mu\text{V/K}$. The reasons for this are two fold. Firstly, Seebeck coefficients below this range do not permit high ZT . Note that the Wiedemann-Franz relation implies that a minimum thermopower of 156 $\mu\text{V/K}$ is necessary for a ZT of unity, and this is for a nil lattice thermal conductivity, which is clearly unrealistic. For example, the thermopower of optimally doped Bi_2Te_3 is approximately 200 $\mu\text{V/K}$ ⁴⁸. Secondly, for thermopower values above 300 $\mu\text{V/K}$, the chemical potential is typically in the band gap, and electrical conductivity is correspondingly reduced due to the low carrier concentration. Since the electrical conductivity we measured in this material is already somewhat low for a high performance thermoelectric (about 1/6th the value for optimized Bi_2Te_3 ⁴⁸), we will take the higher carrier concentration thermopower of 200 $\mu\text{V/K}$ as representing a sample of likely optimal doping.

Our second assumption concerns the thermal conductivity. This may generally be written as a sum of lattice and electronic thermal conductivity. The electronic thermal conductivity $\kappa_{\text{electronic}}$ can be readily estimated from the electrical

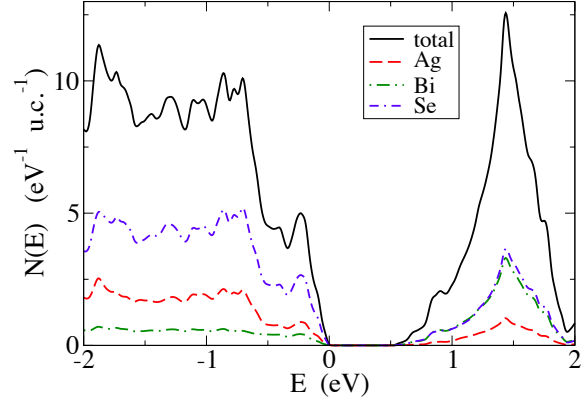


FIG. 8. The calculated density-of-states of AgBiSe_2 .

conductivity σ and the Wiedemann-Franz relation, in which $\kappa_{\text{electronic}} = L_0 \sigma T$, with L_0 the Lorenz number $= 2.45 \times 10^{-8} (\text{V/K})^2$. This relation is usually accurate for metals and heavily doped semiconductors as considered here. The lattice thermal conductivity κ_{lattice} typically follows a $1/T$ relation, leading to an estimation of κ_{lattice} for AgBiSe_2 at 300 K of 0.7 W/m-K.

We also make a final assumption regarding the electrical conductivity, in particular the scattering time. The first principles calculations yield for the n -type sample experimentally measured a σ/τ at 300 K of $2 \times 10^{18} (\Omega \cdot \text{m} \cdot \text{s})^{-1}$, and given the measured conductivity of 160 S/cm, yield an average scattering time τ of $8 \times 10^{-15} \text{s}$. To translate this time to a scattering time for optimally doped p -type requires consideration of two specific issues: the change in carrier type from n -type to p -type, and the change in carrier concentration from the $n = 2.3 \times 10^{19} \text{cm}^{-3}$ in our experimental work to the likely optimal p -type doping $p = 1.2 \times 10^{20} \text{cm}^{-3}$.

Regarding the carrier change from n -type to p -type, one is really asking about the associated difference in electron-phonon coupling, since such coupling is the basic mechanism of resistivity in heavily doped semiconductors above the Debye temperature. To help assess this issue, in Figure 8 we present the calculated density-of-states of AgBiSe_2 . In both the valence and conduction band the Se atoms contribute substantially to the DOS, with the Ag comparatively less in both. The Bi DOS is more substantial in the conduction band than in the valence band. Overall, however, the relative proportions of the partial DOS in the conduction and valence bands are similar - both are substantially hybridized. This suggests that the interatomic interactions which produce the electron-phonon coupling may not be too dissimilar from the conduction and valence bands, and that, as a first approximation, one may take the electron phonon coupling and associated scattering times to be the same for both bands. Hence we may estimate the conductivity and ZT of optimally doped p -type AgBiSe_2 from this scattering time. We find a 300 K conductivity of $800 (\Omega \cdot \text{cm})^{-1}$, approximately 80 percent of the value

of optimally doped Bi_2Te_3 , which yields a 300 K ZT value of 0.7.

At a further level of refinement, we consider that the likely optimal doping level of p -type AgBiSe_2 is substantially higher - more than a factor of five larger - than the experimental carrier concentration in our n -type sample, which may affect carrier mobility. To assess this effect, we examine previous work³⁰ which finds that in the heavily-doped degenerate limit the carrier mobility μ typically follows the approximate relationship $\mu \sim p^{-0.6}$. Taking this same proportionality for the scattering time yields a 300 K conductivity of $300 (\Omega\text{-cm})^{-1}$ and an estimated ZT value of 0.4.

We note that experimental values of ZT will depend on actual scattering times, so that the above should be taken only as first estimates. However, they demonstrate the potential of p -type AgBiSe_2 as a room temperature thermoelectric. In fact, the actual performance of this material may well be better than these estimates, because no effort has been made to model reductions of lattice thermal conductivity as are often attained by alloying or nanostructuring. For example, we may estimate the lattice thermal conductivity of optimally doped Bi_2Te_3 from the Wiedemann-Franz relation, its ZT of unity, and Seebeck coefficient and conductivity of $200 \mu\text{V}/\text{K}$ and⁴⁸ $1000 (\Omega\text{-cm})^{-1}$ as just $0.45 \text{ W}/\text{m}\cdot\text{K}$, which is likely near the minimum possible for this system, and much lower than the $1.7 \text{ W}/\text{m}\cdot\text{K}$ bulk value⁴⁹. We anticipate similar reductions may be available for AgBiSe_2 ; indeed, recent work on AgBiSe_2 nanoplates²³ finds lattice thermal conductivity values of $0.45 \text{ W}/\text{m}\cdot\text{K}$ in the pure material and values as low as half this when Sb alloying is considered.

Appendix B: Demonstration of isotropy of thermopower within effective mass approximation

We here demonstrate directly that an anisotropic effective mass tensor leads to an isotropic Seebeck coefficient, within a single band model constant scattering time approximation (CSTA). Earlier references to this Seebeck isotropy may be found in Refs. 50 and 51. We begin with the anisotropic dispersion relation for a single band extremum within the effective mass approximation (we take $\hbar = 1$ throughout):

$E_{\mathbf{k}} = k_x^2/2m_x + k_y^2/2m_y + k_z^2/2m_z$. Now, equation (4) in Section IV yields a transport function $\sigma_{\alpha\alpha}$:

$$\sigma_{\alpha\alpha} = \tau \int \frac{v_{\alpha,\mathbf{k}}^2}{|v_{\mathbf{k}}|} dS \quad (20)$$

We now make a scale transformation, writing $k_\alpha = \sqrt{2m_\alpha}k'_\alpha$, and convert k'_x, k'_y and k'_z to spherical coordinates. Now, the surface area element dS can easily be shown to be

$$dS = 2E f_1(m_x, m_y, m_z, \theta, \phi) \quad (21)$$

defining an angular function f_1 . Similarly, one finds that

$$|v_{\mathbf{k}}| = \sqrt{E} g_1(m_x, m_y, m_z, \theta, \phi)$$

defining a function g_1 , and

$$v_{\alpha,\mathbf{k}}^2 = 2E n_\alpha^2(\theta, \phi)/m_\alpha \quad (22)$$

where $n_\alpha(\theta, \phi)$ is the direction cosine of k'_α (i.e., $n = \cos(\theta)$ for $\alpha = z$). Now we have

$$\sigma_{\alpha\alpha}(E) = \int v_{\alpha,\mathbf{k}}^2/|v_{\mathbf{k}}| dS = E^{3/2} \int g_{2,\alpha}(m_x, m_y, m_z, \theta, \phi) d\theta d\phi$$

where the function $g_{2,\alpha}$ contains all the angular k' -space dependence and effective mass dependence. The angular integrations yield a third function $g_{3,\alpha}(m_x, m_y, m_z)$ so that we have

$$\sigma_{\alpha\alpha}(E) = E^{3/2} g_{3,\alpha}(m_x, m_y, m_z) \quad (23)$$

However - *and this is the key point* - when inserted into Eq. (1), the effective-mass dependent term $g_{3,\alpha}$ cancels, since it is present both in the numerator and denominator of Eq. (1). Hence the Seebeck coefficient is isotropic, even with an anisotropic effective mass tensor.

Note that although we have assumed the constant scattering time approximation for simplicity, this result holds so long as the scattering time is a function of energy alone, and not direction.

Acknowledgment. This work was supported by the U.S. Department of Energy, Office of Science, Basic Energy Sciences, Materials Sciences and Engineering Division (AFM) and the S3TEC, an Energy Frontier Research Center funded by the U.S. Department of Energy, Office of Science, Basic Energy Sciences (DP and DJS).

¹ N.A. Mecholsky, L. Resca, I.L. Pegg and M. Fornari, "Theory of band warping and its effects on thermoelectronic transport properties." *Phys. Rev. B*, **89**, 155131 (2014).

² A. Shakouri, "Recent developments in semiconductor thermoelectric physics and materials." *Ann. Rev. Mat. Res.* **41**, 399 (2011).

³ X. Chen, D. Parker, and D. J. Singh. "Importance of non-parabolic band effects in the thermoelectric properties of semiconductors." *Sci. Rep.* **3**, 3168 (2013).

⁴ H. Usui, K. Suzuki, K. Kuroki, S. Nakano, K. Kudo, K., and M. Nohara. "Large Seebeck effect in electron-doped FeAs_2 driven by a quasi-one-dimensional pudding-mold-type band", *Phys. Rev. B* **88**, 075140 (2013).

⁵ R. Arita, K. Kuroki, K. Held, A. V. Lukoyanov, S. Skornyakov, and V. I. Anisimov. "Origin of large thermopower in LiRh_2O_4 : calculation of the Seebeck coefficient by the combination of local density approximation and dynamical mean-field theory." *Phys. Rev. B* **78**, 115121 (2008).

⁶ L.D. Hicks and M. S. Dresselhaus. "Effect of quantum-well structures on the thermoelectric figure of merit." *Phys. Rev. B* **47**, 12727 (1993).

⁷ L.D. Hicks and M. S. Dresselhaus. "Thermoelectric figure of merit of a one-dimensional conductor." *Phys. Rev. B* **47**, 16631 (1993).

⁸ D. Parker, X. Chen and D.J. Singh, "High three-dimensional thermoelectric performance from low-dimensional bands", *Phys. Rev.*

- Lett. **110**, 146601 (2013).
- ⁹ Y. Pei, X. Shi, A. LaLonde, H. Wang, L. Chen and G.J. Snyder, "Convergence of electronic bands for high performance bulk thermoelectrics", *Nature* **473**, 66 (2011).
 - ¹⁰ G.D. Mahan, "Good thermoelectrics." *Solid State Physics* **51**, 81(1997).
 - ¹¹ W. Liu, X. Tan, K. Yin, H. Liu, X. Tang, J. Shi, Q. Zhang, and C. Uher. "Convergence of conduction bands as a means of enhancing thermoelectric performance of n-type $\text{Mg}_2\text{Si}_{1-x}\text{Sn}_x$ solid solutions." *Phys. Rev. Lett.* **108**, 166601 (2012).
 - ¹² H. Wang, Y. Pei, A. D. LaLonde, and G. J. Snyder. "Weak electron-phonon coupling contributing to high thermoelectric performance in n-type PbSe." *Proc. National Acad. Sci.* **109**, 9705 (2012).
 - ¹³ J.R. Sootsman, D.Y. Chung, and M.G. Kanatzidis, M. G. , "New and old concepts in thermoelectric materials", *Angew. Chem. Int. Ed.* **48**, 8616-8639 (2009)
 - ¹⁴ M.S. Lee, F. P. Poudeu, and S. D. Mahanti. "Electronic structure and thermoelectric properties of Sb-based semiconducting half-Heusler compounds." *Phys. Rev. B* **83** 085204 (2011).
 - ¹⁵ F.J. DiSalvo, "Thermoelectric cooling and power generation." *Science* **285**, 703 (1999).
 - ¹⁶ G. Wang and T. Cagin. "Electronic structure of the thermoelectric materials Bi_2Te_3 and Sb_2Te_3 from first-principles calculations." *Phys. Rev. B* **76**, 075201 (2007).
 - ¹⁷ H. Ohta, K. Sugiura, and K. Koumoto, "Recent Progress in Oxide Thermoelectric Materials: *p*-Type $\text{Ca}_3\text{Co}_4\text{O}_9$ and *n*-Type SrTiO_3 ." *Inorg. Chem.* **47**, 8429 (2008).
 - ¹⁸ G.J. Snyder and E. S. Toberer. "Complex thermoelectric materials." *Nat. Mat.* **7**, 105 (2008).
 - ¹⁹ A.D. LaLonde, Y. Pei, H. Wang, and G. J. Snyder. "Lead telluride alloy thermoelectrics." *Mat. Today* **14**, 526 (2011).
 - ²⁰ M. Stordeur, M. Stlzer, H. Sobotta and V. Riede, "Investigation of the valence band structure of thermoelectric $(\text{Bi}_{1-x}\text{Sb}_x)_2\text{Te}_3$ single crystals. *Physica Stat. Sol.* **150**, 165 (1988).
 - ²¹ K.F. Cuff, M.K. Ellet, C.D. Kulgin, L.R. Williams, *Proc. Int. Conf. Phys. Semicond. Paris 1964*, 677.
 - ²² L. Pan, D. Brardan, and N. Dragoe. "High thermoelectric properties of *n*-type AgBiSe_2 ." *J. Am. Chem. Soc.* **135**, 4914 (2013).
 - ²³ C. Xiao, J. Xu, B. Cao, K. Li, M. Kong, and Y. Xie, "Solid-solutioned homojunction nanoplates with disordered lattice: A promising approach toward 'Phonon Glass Electron Crystal' thermoelectric materials", *J. Am. Chem. Soc.* **134**, 7971-7977 (2012)..
 - ²⁴ C. Xiao, X. Qin, J. Zhang, R. An, J. Xu, K. Li, B. Cao, J. Yang, B. Ye and Y. Xie, "High thermoelectric and reversible pnp conduction type switching integrated in dimetal chalcogenide", *J. Am. Chem. Soc.* **134**, 18460-18466 (2012).
 - ²⁵ United States Geological Survey Minerals Information 2015, available at <http://minerals.usgs.gov/minerals/pubs/commodity/>.
 - ²⁶ D.R. Lide (ed.) *CRC Handbook of Chemistry and Physics*, Section 14 (CRC Press: Boca Raton), 2005.
 - ²⁷ T. Sakakibara, Y. Takigawa, and K. Kurosawa. "Hall Mobility Enhancement in AgBiTe_2 - Ag_2Te Composites." *Japanese J. of Appl. Physics* **41**, 2842 (2002).
 - ²⁸ A.E. White, K. T. Short, and D. J. Eaglesham. "Electrical and structural properties of $\text{Si}/\text{CrSi}_2/\text{Si}$ heterostructures fabricated using ion implantation." *Appl. Phys. Lett.* **56**, 1260 (1990)
 - ²⁹ Y.S. Hor, A. Richardella, P. Roushan, Y. Xia, J. G. Checkelsky, A. Yazdani, M. Z. Hasan, N. P. Ong, and R. J. Cava. "*p*-type Bi_2Se_3 for topological insulator and low-temperature thermoelectric applications." *Phys. Rev. B* **79**, 195208 (2009).
 - ³⁰ D. Parker and D. J. Singh. "High-temperature thermoelectric performance of heavily doped PbSe." *Physical Review B* **82**, 035204 (2010).
 - ³¹ M.D Nielsen, V. Ozolins, and J. P. Heremans. "Lone pair electrons minimize lattice thermal conductivity." *Energy and Env. Sci.* **6**, 570 (2013).
 - ³² P. B. Allen, "Empirical electron-phonon λ values from resistivity of cubic metallic elements." *Physical Review B* **36**, 2920 (1987).
 - ³³ H. Shi, D. Parker, M.-H. Du, and D. J. Singh. "Connecting thermoelectric performance and topological-insulator behavior: Bi_2Te_3 and $\text{Bi}_2\text{Te}_2\text{Se}$ from First Principles." *Phys. Rev. Appl.* **3**, 014004 (2015).
 - ³⁴ Note that in this calculation of m_σ for Bi_2Te_3 we are assuming the use of a polycrystalline sample for which the effective conductivity mass m_σ is given by $3/m_\sigma = 1/m_1 + 1/m_2 + 1/m_3$. The DOS mass m_{DOS} is unchanged by the use of a polycrystalline sample.
 - ³⁵ K. Biswas, J. He, I.D. Blum, C. I. Wu, T.P. Hogan, D.N. Seidman, V.P. Dravid and M.G Kanatzidis, "High-performance bulk thermoelectrics with all-scale hierarchical architectures". *Nature* **489**, 414 (2012).
 - ³⁶ L. Zhang and D. J. Singh. "Electronic structure and thermoelectric properties of layered PbSe- WSe_2 materials." *Phys. Rev. B* **80**, 075117 (2009).
 - ³⁷ H.J. Goldsmid, "Application of the transverse thermoelectric effects", *J. Elec. Mat.* **40**, 1254 (2011).
 - ³⁸ N.W. Ashcroft and N.D. Mermin, *Solid State Physics*, (Thomson Learning: 1976), p. 251.
 - ³⁹ P. Blaha, K. Schwarz, G. Madsen, D. Kvasnicka and J. Luitz, WIEN2k, An Augmented Plane Wave + Local Orbitals Program for Calculating Crystal Properties (K. Schwarz, Tech. Univ. Wien, Austria, 2001).
 - ⁴⁰ G.K.H. Madsen and D. J. Singh. "BoltzTraP. A code for calculating band-structure dependent quantities." *Comp. Phys. Comm.* **175**, 67(2006).
 - ⁴¹ J.P. Perdew, K. Burke, and M. Ernzerhof, "Generalized gradient approximation made simple", *Phys. Rev. Lett.* **77** , 3865 (1996).
 - ⁴² F. Tran, and P. Blaha. "Accurate band gaps of semiconductors and insulators with a semilocal exchange-correlation potential." *Phys. Rev. Lett.* **102**, 226401 (2009).
 - ⁴³ D. Koller, F. Tran, and P. Blaha. "Merits and limits of the modified Becke-Johnson exchange potential." *Phys. Rev. B* **83**, 195134 (2011).
 - ⁴⁴ D.J. Singh, "Electronic structure calculations with the Tran-Blaha modified Becke-Johnson density functional." *Phys. Rev. B* **82**, 205102 (2010).
 - ⁴⁵ M. Lax, *Symmetry principles in solid state and molecular physics*, Courier Dover Publications, 1974.
 - ⁴⁶ D.T. Morelli, V. Jovovic, and J. P. Heremans. "Intrinsically minimal thermal conductivity in cubic I-V-VI₂ semiconductors." *Phys. Rev. Lett.* **101**, 035901 (2008).
 - ⁴⁷ W. E. Bies, R. J. Radtke, H. Ehrenreich, and E. Runge. "Thermoelectric properties of anisotropic semiconductors." *Phys. Rev. B* **65**, 085208 (2002).
 - ⁴⁸ G.S. Nolas, J. Sharp, and H. J. Goldsmid, *Thermoelectrics: basic principles and new materials developments*. Vol. 45. Springer, 2001.
 - ⁴⁹ D.M. Rowe, ed. *CRC Handbook of Thermoelectrics*, CRC Press: Boca Raton, 1995.
 - ⁵⁰ B.S. Chandrasekhar, "The Seebeck coefficient of Bismuth single crystals." *J. Phys. Chem. Sol.* **11**, 268 (1959).
 - ⁵¹ J. Kolodziejczak and S. Zukotynski, "Galvano- and thermomagnetic effects in semiconductors with non-spherical and non-parabolic energy bands." *Phys. Stat. Sol.* **5**, 145 (1964).